

The dynamic energy balance in earthquakes expressed by fault surface morphology

Xin Wang^{a,*}, Juan Liu^a, Feng Gao^a, Zhizhen Zhang^a

^aState Key Laboratory for Geomechanics and Deep Underground Engineering, China University of Mining and Technology, Xuzhou 221116, China

Abstract

The dynamic energy balance is essential for earthquake studies. The energy balance approach is one of the most famous developments in fracture mechanics. To interpret seismological data, crack models and sliding on a frictional surface (fault) models are widely used. The macroscopically observable energy budget and the microscopic processes can be related through the fracture energy G_c . The fault surface morphology is the direct result of the microscopic processes near the crack tip or on the frictional interface. Here we show that the dynamic energy balance in earthquakes can be expressed by fault surface morphology, and that they are quantitatively linked. The direct shear experiments proves the predictions of the theoretical discussions, and show that the strain rate has crucial influence on the dynamic energy balance.

Keywords:

Earthquakes; Dynamic energy balance; Surface morphology; Strain rate

1. Introduction

An earthquake may be considered to be a dynamically running shear crack (Scholz, 2019), in which the dynamic energy balance is essential for earthquake studies. In the field of fracture mechanics, the energy balance approach employed by Griffith has become one of the most famous developments in materials science (Collins, 1993). To interpret seismological data, crack models are often used in part because the theories on cracks have been developed well. On the other hand, seismic faulting may be more intuitively viewed

*Corresponding author

Email address: ericrussell@zju.edu.cn (Xin Wang)

as sliding on a frictional surface (fault) where the physics of friction, especially stick slip, plays a key role.

The fracture energy, G_c , in crack theory is the energy needed to create new crack surfaces near the crack tip. Thus, the system must expend the threshold fracture energy G_c before the crack can extend. In contrast, in frictional sliding model, D_c , is introduced as a critical slip before rapid sliding begins at a constant friction. If the initial stress σ_0 of the system drops more or less linearly to the final stress σ_1 , i.e., the final value of the frictional stress σ_f , the energy spent in the system before this happens can be approximately written as $\frac{1}{2}(\sigma_0 - \sigma_1)D_c$. Thus, if we are to link a crack model to a friction model, we can equate this energy to G_c , i.e., $G_c = \frac{1}{2}(\sigma_0 - \sigma_1)D_c$. Then we can relate the macroscopically observable energy budget to the microscopic processes in a surprisingly general way. Any constraint on fracture energy obtained from the energy budget will provide a strong bound on all microscopic rupture processes (Kanamori and Brodsky, 2004). Svetlizky and Fineberg (2014) have shown that interface rupture propagation is described by, essentially, the same framework of the crack model. This suggests that an analogous 'Griffith' condition may exist for the onset of rupture propagation for a frictional interface.

The fault surface morphology is the direct result of the microscopic processes near the crack tip or on the frictional interface. Here we show that the dynamic energy balance in earthquakes can be expressed by fault surface morphology, and that they are quantitatively linked.

2. The description of fault surface morphology and its links to the dynamic energy balance in earthquakes

The description of fault surface morphology has been investigated in the literature (e.g., Ladanyi and Archambault, 1969; Barton and Choubey, 1977; Plesha, 1987; Saeb and Amadei, 1992; Amadei et al., 1998) while trying to study the contribution of surface morphology to the shear strength of rock fractures. As shearing strictly depends on three-dimensional contact area location and distribution (Gentier et al., 2000), Grasselli et al. (2002) proposed a method for the quantitative three-dimensional description of a rough fracture surface, and based on this description, Grasselli and Egger (2003) proposed a

constitutive criterion to model the shear strength of fractures. Wang et al. (2019) defined the terms “quasi steps” and “quasi striations” to refer to morphological structures that are created during the creation of new crack surfaces and the friction on the frictional interface. The same morphological structures are also causing anisotropy of the fracture surface morphology, hence the anisotropy of the surface morphology’s contribution on its shear strength. The terms “quasi steps” and “quasi striations” are broader definitions of the fault steps and fault striations whether they can be obviously seen or not. The parameter θ_{max}^*/C was proposed by Grasselli et al. (2002) to describe the contribution of fracture surface morphology on the shear strength. Wang et al. (2019) proposed a theoretical model that describes the contribution of quasi steps and quasi striations on the shear strength. And by fitting this theoretical model to θ_{max}^*/C from each slip direction on the fracture surface, the amount of quasi steps R_G and quasi striations R_H can be estimated. Combined with the method proposed by Wang et al. (2017) for outcrop fracture surface extraction from point cloud data, the estimated quasi steps and quasi striations data had good applications in tectonics (e.g., Wang and Gao, 2020).

Let’s consider the formation of quasi steps during the crack growth. The voids (Fig. 1 as suggested by Bouchaud and Paun (1999)) are nucleated under the influence of the stress field adjacent to the tip, but not at the tip, due to the existence of the plastic zone that cuts off the purely linear-elastic (unphysical) crack-tip singularities. The crack grows by coalescing the voids with the tip, creating a new stress field which induces the nucleation of new voids (Bouchbinder et al., 2004). The morphological structures of quasi steps are then formed during the crack growth under shear load as illustrated in Fig. 1. A crucial aspect of this picture is the existence of a typical scale, ξ_c , which is roughly the distance between the crack tip and the first void, at the time of the nucleation of the latter. In this picture there exists a “energy dissipation zone ” in front of the crack tip in which plastic yield is accompanied by the evolution of damage cavities. From this picture, it can also be seen that the typical scale ξ_c is positively related with the estimated amount of quasi steps R_G since the quasi steps are more developed on the fracture surface with larger value of ξ_c .

A simple model for ξ_c was developed (Bouchbinder et al., 2004; Afek et al., 2005) by assuming the energy dissipation zone to be properly described by the Huber–von Mises plas-

ticity theory. The material yields as the distortional energy exceeds a material-dependent threshold σ_Y^2 and the typical distance ξ_c scales as (Bouchbinder et al., 2004)

$$\xi_c \sim \frac{K_{II}^2}{\sigma_Y^2}, \quad (1)$$

where K_{II} is the stress intensity factor for mode II (in-plane shear) cracks. On the other hand, the linear-elastic solution is still valid outside the energy dissipation zone, and the energy release rate G^* can be expressed as

$$G^* = \frac{K_{II}^2}{E'}, \quad (2)$$

where E' is related to Young's modulus E and Poisson's ratio ν (for plane strain):

$$E' = \frac{E}{1 - \nu^2}.$$

The definition of the energy release rate G^* is

$$G^* = \frac{\partial \Omega}{\partial s}, \quad (3)$$

where Ω is the strain energy and s is the crack growth area. Then Eq. 1 can be rewritten as

$$\xi_c \sim G^* / \frac{\sigma_Y^2}{E'} = \frac{\partial \Omega}{\partial s} / \frac{\sigma_Y^2}{E'}. \quad (4)$$

The amount of quasi steps R_G is a description of the degree of quasi steps development over the fracture surface, so it is an average quantity over the fracture surface. R_G should scale with $\overline{\xi_c}$, the average of ξ_c over the fracture surface S :

$$R_G \sim \overline{\xi_c} = \frac{1}{S} \int_s \xi_c \sim \frac{\Omega}{\gamma_G}, \quad (5)$$

where

$$\gamma_G = \int_S \frac{\sigma_Y^2}{E'}. \quad (6)$$

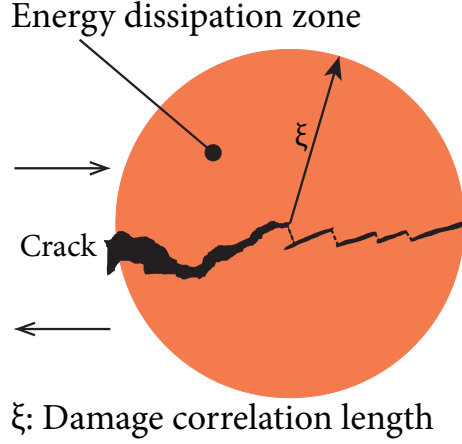


Figure 1: The model of the tip growth of mode II (in-plane shear) cracks. The formation of voids are documented in [Bouchaud and Paun \(1999\)](#).

Let's consider the formation of quasi striations during the friction on the frictional interface. As suggested by [Svetlizky and Fineberg \(2014\)](#), the interface rupture friction is described by, essentially, the same framework of the crack model. The main difference is that the crack model consider the crack growth in the rock mass, while the friction model consider the crack growth through the local protruding obstacles on the frictional interface, which are then removed or deformed during the friction. As the slip goes on, more protruding obstacles that face the slip direction with high angles are removed or deformed while protruding obstacles that are high angle perpendicular to the slip direction are kept. This anisotropy results in the macroscopic quasi striations structures. The amount of quasi striations R_H is a description of the degree of quasi striations development over the fracture surface, so it is an average quantity over the fracture surface. R_H should scale with E_f , the frictional energy like this:

$$R_H \sim \frac{E_f}{\bar{\omega}}, \quad (7)$$

where $\bar{\omega}$ is the average strain energy needed to remove or deform a protruding obstacle. Suppose n protruding obstacles are removed or deformed, according to Eq. 5 and Eq. 6, the strain energy scale as

$$\omega_1 \sim \int_{S_1^*} \frac{\sigma_Y^2}{E'}, \omega_2 \sim \int_{S_2^*} \frac{\sigma_Y^2}{E'}, \dots, \omega_n \sim \int_{S_n^*} \frac{\sigma_Y^2}{E'},$$

where S_i^* is the crack area in the i -th protruding obstacle. The average strain energy $\bar{\omega}$ can be written as

$$\bar{\omega} = \frac{1}{n} \sum \omega_i \sim \int \overline{\left(\frac{\sigma_Y^2}{E'}\right)}, \quad (8)$$

where

$$\bar{S}^* = \frac{1}{n} \sum S_i^*,$$

and

$$\overline{\left(\frac{\sigma_Y^2}{E'}\right)} = \sum \int_{S_i^*} \frac{\sigma_Y^2}{E'} / \sum S_i^*.$$

Finally, we have the link between the fault surface morphology and the dynamic energy balance in earthquakes:

$$\frac{R_G}{R_H} \sim \frac{\bar{\omega}}{\gamma_G} \frac{\Omega}{E_f}. \quad (9)$$

3. The experimental results and discussions

An experiment was designed to test the above theoretical discussion. The dimensions and experiment settings are illustrated in Fig. 2. 14 red sandstone rock samples are tested in this simple direct shear experiment with the strain rate ranging from 0.01/min to 0.083/min. The final fracture surfaces after the crack growth and the interface friction processes are scanned and analyzed, the amount of quasi steps R_G and quasi striations R_H are estimated. On the other hand, the stress-strain curves are recorded during the tests. As shown in Fig. 3, the strain energy is mainly accumulated before the formation of the macroscopic crack through the rock sample, while the frictional energy is mainly spent after the formation of the macroscopic crack. Thus the strain energy Ω and the frictional energy E_f can be roughly estimated.

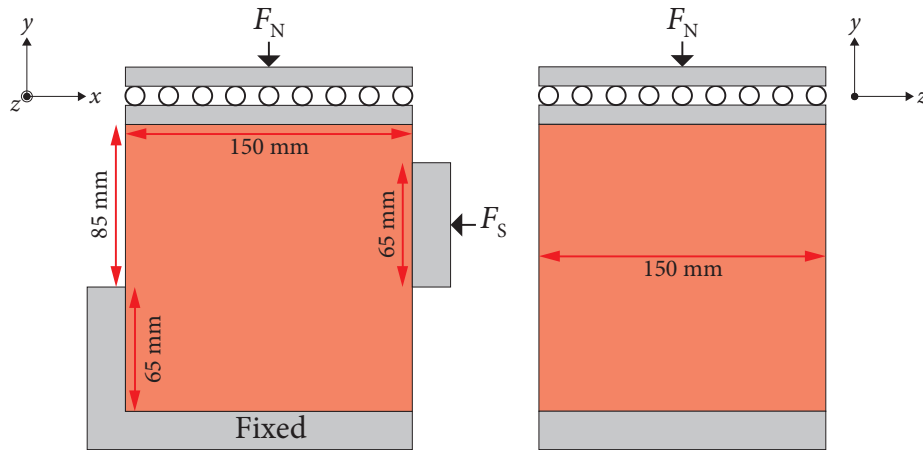


Figure 2: Experiment settings of direct shear test.

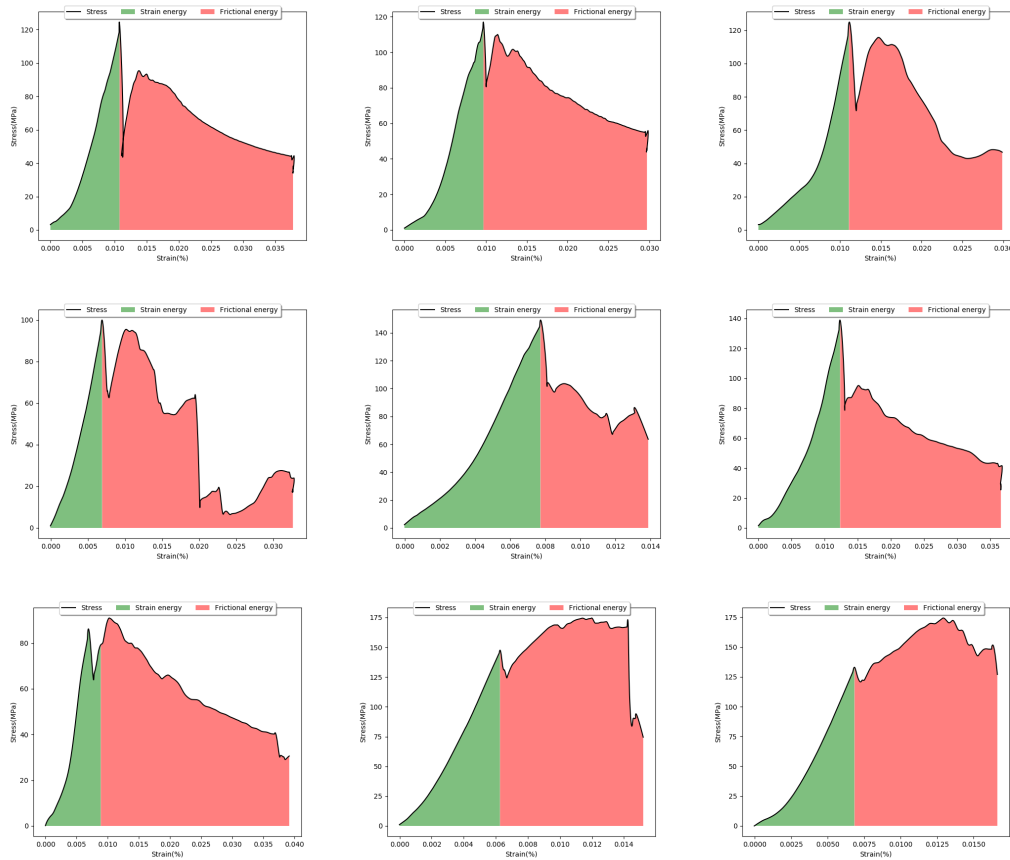


Figure 3: Examples of the stress-strain curve. Roughly the green regions represent the strain energy to be released during the crack growth, and the red regions represent the frictional energy spent during the friction on the frictional interface.

The rock samples are numbered and their strain rate during the test are shown in Table 1. The ratio between the amount of quasi steps and the amount of quasi striations (R_G/R_H) is plotted against $\log(\Omega)/\log(E_f)$. The logarithm of the strain energy and the frictional energy are taken here in order to compare their values with R_G and R_H , although the logarithm relationship is not explicitly shown in above discussions (e.g., Eq. 5 and Eq. 7). Results of rock samples are scatter plotted in Fig. 4 with their sample numbers labeled on their corresponding scatter points for reference.

Table 1: Rock sample numbers and their strain rate during the test.

Sample N.O.	0	1	2	3	4	5	6
Strain rate (%/min)	0.08	0.077	0.07	0.063	0.037	0.03	0.01
Sample N.O.	7	8	9	10	11	12	13
Strain rate (%/min)	0.017	0.023	0.033	0.043	0.057	0.067	0.083

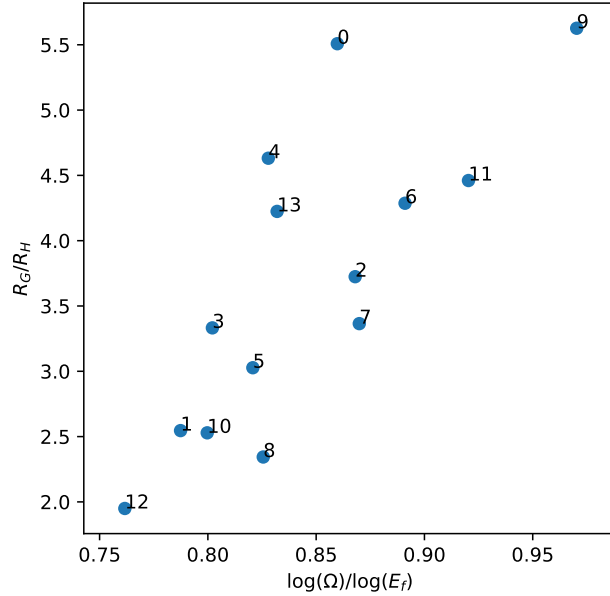


Figure 4: The experimental results. The ratio between the amount of quasi steps and the amount of quasi striations (R_G/R_H) is plotted against $\log(\Omega)/\log(E_f)$. Each labeled point is the result of the corresponding rock sample, and its strain rate can be found in Table 1.

The results show that there seems indeed a quantitative link between the fault surface morphology and the dynamic energy balance in earthquakes as theoretically predicted above. Some of the scattered results show a constant value of $\bar{\omega}/\gamma_G$ (e.g., sample number 12, 1, 10, 5, 2, 6, 11 and 9) because $\bar{\omega}$ and γ_G are both integrals of σ_Y^2/E' over some area, whose average tend to be the same for the same rock sample, although it varies locally. Thus the link predicted by Eq. 9 has the property of material-independent, at least for dry brittle materials discussed here.

Note that sample number 3, 13, 4 and 0 seem have slightly larger value of $\bar{\omega}/\gamma_G$, and they seem have larger strain rate. On the contrary, sample number 7 and 8 have slightly smaller value of $\bar{\omega}/\gamma_G$ and they have smaller strain rate. If we take the rupture speed V into account, Eq. 9 becomes

$$\frac{R_G}{R_H} \sim \frac{\bar{\omega}(1 - \frac{V^2}{(B\beta)^2})}{\gamma_G} \frac{\Omega}{E_f}, \quad (10)$$

where B is a constant of the order of 1 and β is the shear-wave speed (Kanamori and Brodsky, 2004), because

$$G = G^* g(V) = \frac{\partial \Omega}{\partial s} (1 - \frac{V^2}{(B\beta)^2}).$$

But this doesn't explain the data and the rupture speeds V aren't significantly different in those tests, so the rupture speeds V doesn't have a significant effect here. One explanation is that for real materials, σ_Y^2 depends on the state of deformation and its history. Experiments discussed here show that high strain rate results in larger value of $\bar{\omega}$, i.e., on average, it needs more energy to remove or deform a protruding obstacle on the fracture surface during the friction. In the formation of the macroscopic crack and the protruding obstacles on the crack surface, high strain rate may make less plastic deformation inside the protruding obstacles, and hence more energy is needed to remove or deform them in the following deformation.

4. Conclusions

The dynamic energy balance is essential for earthquake studies. To interpret seismological data, crack models and sliding on a frictional surface (fault) models are widely used.

From these two types of models, the macroscopically observable energy budget and the microscopic processes can be related through the fracture energy G_c .

The fault surface morphology is the direct result of the microscopic processes near the crack tip or on the frictional interface. Here we show that the dynamic energy balance in earthquakes can be expressed by fault surface morphology, and that they are quantitatively linked.

The direct shear experiments proves the predictions of the theoretical discussions, and show that the strain rate has crucial influence on the dynamic energy balance. The link predicted by the theoretical discussions has the property of material-independent, at least for dry brittle materials discussed here.

Acknowledgments

This research was funded by the Fundamental Research Funds for the Central Universities (grant no. 2020QN29), the China Postdoctoral Science Foundation (Grant no. 2020M681759), and the State Key Program of National Natural Science Foundation of China (Grant no. 51934007).

References

- Afek, I., Bouchbinder, E., Katzav, E., Mathiesen, J., Procaccia, I., 2005. Void formation and roughening in slow fracture. *Physical Review E* 71, 066127. doi:[10.1103/PhysRevE.71.066127](https://doi.org/10.1103/PhysRevE.71.066127).
- Amadei, B., Wibowo, J., Sture, S., Price, R.H., 1998. Applicability of existing models to predict the behavior of replicas of natural fractures of welded tuff under different boundary conditions. *Geotechnical & Geological Engineering* 16, 79–128. doi:[10.1023/A:1008886106337](https://doi.org/10.1023/A:1008886106337).
- Barton, N., Choubey, V., 1977. The shear strength of rock joints in theory and practice. *Rock mechanics* 10, 1–54. doi:[10.1007/BF01261801](https://doi.org/10.1007/BF01261801).
- Bouchaud, E., Paun, F., 1999. Fracture and damage at a microstructural scale. *Computing in Science Engineering* 1, 32–38. doi:[10.1109/5992.790585](https://doi.org/10.1109/5992.790585).

- Bouchbinder, E., Mathiesen, J., Procaccia, I., 2004. Roughening of fracture surfaces: The role of plastic deformation. *Physical Review Letters* 92, 245505. doi:[10.1103/PhysRevLett.92.245505](https://doi.org/10.1103/PhysRevLett.92.245505).
- Collins, J.A., 1993. *Failure of materials in mechanical design: analysis, prediction, prevention*. John Wiley & Sons.
- Gentier, S., Riss, J., Archambault, G., Flamand, R., Hopkins, D., 2000. Influence of fracture geometry on shear behavior. *International Journal of Rock Mechanics and Mining Sciences* 37, 161 – 174. doi:[10.1016/S1365-1609\(99\)00096-9](https://doi.org/10.1016/S1365-1609(99)00096-9).
- Grasselli, G., Egger, P., 2003. Constitutive law for the shear strength of rock joints based on three-dimensional surface parameters. *International Journal of Rock Mechanics and Mining Sciences* 40, 25 – 40. doi:[10.1016/S1365-1609\(02\)00101-6](https://doi.org/10.1016/S1365-1609(02)00101-6).
- Grasselli, G., Wirth, J., Egger, P., 2002. Quantitative three-dimensional description of a rough surface and parameter evolution with shearing. *International Journal of Rock Mechanics and Mining Sciences* 39, 789 – 800. doi:[10.1016/S1365-1609\(02\)00070-9](https://doi.org/10.1016/S1365-1609(02)00070-9).
- Kanamori, H., Brodsky, E.E., 2004. *The physics of earthquakes*. *Reports on Progress in Physics* 67, 1429–1496. doi:[10.1088/0034-4885/67/8/r03](https://doi.org/10.1088/0034-4885/67/8/r03).
- Ladanyi, B., Archambault, G., 1969. Simulation of shear behavior of a jointed rock mass, in: *The 11th US Symposium on Rock Mechanics (USRMS)*, American Rock Mechanics Association.
- Plesha, M.E., 1987. Constitutive models for rock discontinuities with dilatancy and surface degradation. *International Journal for Numerical and Analytical Methods in Geomechanics* 11, 345–362. doi:[10.1002/nag.1610110404](https://doi.org/10.1002/nag.1610110404).
- Saeb, S., Amadei, B., 1992. Modelling rock joints under shear and normal loading. *International Journal of Rock Mechanics and Mining Sciences & Geomechanics Abstracts* 29, 267 – 278. doi:[10.1016/0148-9062\(92\)93660-C](https://doi.org/10.1016/0148-9062(92)93660-C).
- Scholz, C.H., 2019. *The Mechanics of Earthquakes and Faulting*. 3 ed., Cambridge University Press. doi:[10.1017/9781316681473](https://doi.org/10.1017/9781316681473).

- Svetlizky, I., Fineberg, J., 2014. Classical shear cracks drive the onset of dry frictional motion. *Nature* 509, 205–208. doi:[10.1038/nature13202](https://doi.org/10.1038/nature13202).
- Wang, X., Gao, F., 2020. Quantitatively deciphering paleostrain from digital outcrops model and its application in the eastern tian shan, china. *Tectonics* 39, e2019TC005999. doi:[10.1029/2019TC005999](https://doi.org/10.1029/2019TC005999).
- Wang, X., Qin, Y., Yin, Z., Zou, L., Shen, X., 2019. Historical shear deformation of rock fractures derived from digital outcrop models and its implications on the development of fracture systems. *International Journal of Rock Mechanics and Mining Sciences* 114, 122–130. doi:[10.1016/j.ijrmms.2018.12.018](https://doi.org/10.1016/j.ijrmms.2018.12.018).
- Wang, X., Zou, L.J., Shen, X.H., Ren, Y.P., Qin, Y., 2017. A region-growing approach for automatic outcrop fracture extraction from a three-dimensional point cloud. *Computers & geosciences* 99, 100–106. doi:[10.1016/j.cageo.2016.11.002](https://doi.org/10.1016/j.cageo.2016.11.002).